

1 **Manuscript Number** : amt-2017-250  
2 **Associate Editor** : Dr. Jens Wickert  
3 **Manuscript Title** : Comparisons of the tropospheric specific humidity from GPS radio  
4 occultations with ERA-Interim, NASA MERRA and AIRS data  
5

6 **Dear Referee #1,**  
7

8 We would like to thank reviewer #1 for taking the time to review our manuscript. We greatly  
9 appreciate all comments, which we address and implement in the revised manuscript. The  
10 manuscript has now become stronger and presents additional results for discussion reflecting the  
11 reviewer's comments.  
12

13 **General Comment #1:** The paper is long and it is a little difficult and tiresome to read because  
14 there are three regions and these are discussed in great detail with two figures and one table for  
15 each region. All of this takes 16 pages and the reader may get lost. Perhaps the number of  
16 regions could be reduced to two? It is not clear to me that the difference between +/- 15NS and  
17 15-30NS are important. I become lost in the details of all these comparisons.  
18

19 **Answer:** Agreed. However the 500 hPa and 400 hPa show the same behavior in all three regions.  
20 The only difference is found at the 700 hPa and 600 hPa, which are most influenced by  
21 convection. Thus, although we agree that analyzing three different regions is tiresome, we want  
22 to be inclusive and decided not to merge the results from the +/- 15NS and 15-30NS regions into  
23 one. This is because we would have missed seeing the different behavior of the data at 700 hPa  
24 and 600 hPa in the two regions. However, we took the following actions to make the results  
25 easier to read:  
26

27 **Actions taken:**

- 28 1. We only show the monthly zonal mean time series of the specific humidity and their  
29 interannual anomalies and the accompanied table for the deep tropics (+/- 15NS) and  
30 moved the rest of the figures and tables into the supplementary material. However, we  
31 kept their discussion in the text.  
32
- 33 2. We written more concisely the analysis for each region and avoided repetitive discussion  
34 at 500 hPa and 400 hPa pressure levels, focusing only in the lower troposphere.  
35

---

36  
37 **General Comment #2:** Most importantly, because a major point of the paper is a comparison of  
38 the JPL and UCAR retrievals of specific humidity it is worth mentioning in the abstract the  
39 significant difference between the JPL and UCAR estimation of  $q$  given refractivity  $N$ . JPL uses  
40 a "simple" method (using  $T$  from ECMWF TOGA database in Eq. 1) while UCAR uses a  
41 1DVAR method (using ERA-Interim for the a priori). This difference between these two  
42 methods is likely the main reason for the different results, and not a property of RO in general.  
43 This reason should be verified by also comparing the JPL and UCAR refractivities that were  
44 used in computing  $q$ .  
45

46 **Answer:** The reviewer is correct.

47 **Actions taken:**

48 1. We added relevant text in the manuscript to explicitly state this.  
49 **See Abstract lines 31–33, and lines 148–153.**

50

51 2. We performed additional data processing and data analysis for the refractivity  
52 climatologies and included the results in the manuscripts in a new section and discussion.  
53 **See new Section 3.4.**

54

55

56

57 **General Comment #3:** Finally, it would be helpful if the authors could say something about  
58 what all these differences mean in terms of accuracy of water vapor compared to the estimates of  
59 accuracy in q from other papers. Perhaps this discussion could go in the conclusions.

60 **Answer: Done.** We included background information about the accuracy of RO q retrievals and  
61 compare them with the accuracy of other data sets. Based on this discussion, we explicitly  
62 discuss about the statistical significance of our results throughout the manuscript (when  
63 comparing the different climatologies). **See new added Section 3.4 and lines 235–236.**

---

64

65

66

67 **Specific Comment #1:** SH is not a common abbreviation for specific humidity. I suggest using  
68 the more common letter “q”.

69 **Answer:** Agreed. We removed the abbreviation SH from the manuscript. Instead, we explicitly  
70 write “specific humidity”.

---

71

72

73 **Specific Comment #2:** Line 32. Something is missing here? “as well as” perhaps?

74

75

76 **Answer: Done. Sentence was modified. No need to act on this any more.**

---

77

78

79 **Specific Comment #3:** Page 10, lines 206 – 215. The quoted accuracies of 10-20% below 7 km  
80 and 0.1 g/kg seem inconsistent. For a typical lower tropospheric q of 5-10 g/kg, an error of 0.1  
81 g/kg (1-2%) is far better than 10% (1-2%). The JPL quoted accuracies of 0.2-0.4 g/kg in the  
82 tropics (2-4% for a typical value of q of 10 g/kg) are also very high compared to the quoted  
83 values of 20% for MERRA and 25% for AIRS. Can the authors comment on these large  
84 differences? In general, it is very important for this paper to precisely define previous studies of  
85 the accuracy of water vapor (specific humidity) estimates from RO.

86

87

88 **Answer: Done.** We devoted a separate section establishing the RO specific humidity accuracies  
89 based on previous studies. **See Section 2.6**

---

93 **Specific Comment #4:** It would be helpful to know why the author's study extends downward  
94 only to 700 hPa? Most of the atmospheric water vapor is below 700 hPa. Yes, there is negative N  
95 bias associated with super-refraction and other issues in the lower troposphere, but still it is  
96 important to characterize the errors in retrieved q in this region.  
97

98 **Answer:** This is the same comment with that of Reviewer #2 Minor Comment #5. The reason is  
99 exactly what the reviewer mentions above. Also, the spherical symmetry approximation and  
100 signal tracking issues could also play a role here. In this preliminary climatology analysis, we  
101 wanted to focus on the pressure range that we are confident the RO humidity is well established,  
102 and then we would focus on the boundary layer and higher up in the troposphere. **We have**  
103 **added relevant text to clarify this.** See lines 121–127 and Conclusion section.  
104

---

105  
106  
107  
108 **Specific Comment #5:** The Vergados et al. 2016 paper is in the list of references, but I could not  
109 find it mentioned in the paper.  
110

111 **Answer: Done.** We removed the references.  
112

---

113  
114  
115 **Specific Comment #6:** Lines 285–287. It says that the wet bias in JPL-RO may be due to the  
116 warm bias in the ERA-Interim (We. 1). But they use ECMWF TOGA analysis for the T in Eq. 1,  
117 not the ERA-Interim (lines 150–151). Please clarify. Similarly, lines 420–422 say the JPL  
118 retrieval technique uses "ECMWF" as a-priori temperature information. What ECMWF, TOGA  
119 or Interim?  
120

121 **Answer: Done.** See line 165 and lines 495–500.  
122

---

123  
124  
125  
126 **Specific Comment #7:** Figure 3 is not referred to in text. It looks like it should be in line 291,  
127 i.e. "...we estimate the respective SH anomalies (Figure 3)."  
128

129 **Answer: Done.** Due to re-arranging the figures, Figure 3 now shows the specific humidity  
130 anomalies at the deep tropics and is discussed throughout the manuscript.  
131

---

132  
133  
134 **Specific Comment #8:** Lines 372–373. I suggest rewording to "...defines the subtropics where  
135 dry air descends from the Hadley cell."  
136

137 **Answer: Done.** See lines 423–424.  
138

---

139 **Specific Comment #9:** Lines 474-475. Reword to say “moistest of all data sets” and “driest of  
140 all datasets”.

141  
142 **Answer:** Done. See lines 519–520.  
143 -----

144  
145  
146  
147 **Specific Comment #10:** Lines 490-492: All the pressure levels lie above the PBL not just the  
148 700 hPa level. Do the authors mean that the 700 hPa level is the closest to the PBL?  
149

150 **Answer:** Yes. Please, see modified lines 522–523.  
151 -----

152  
153  
154  
155  
156  
157  
158  
159  
160  
161  
162  
163  
164  
165  
166  
167  
168  
169  
170  
171  
172  
173  
174  
175  
176  
177  
178  
179  
180  
181  
182

183 *Panagiotis Vergados*  
184 **THIS IS THE END OF REVIEWER #1 REPORT .....**

185 **Manuscript Number** : amt-2017-250  
186 **Associate Editor** : Dr. Jens Wickert  
187 **Manuscript Title** : Comparisons of the tropospheric specific humidity from GPS radio  
188 occultations with  
189 ERA-Interim, NASA MERRA and AIRS data  
190

191 **Dear Referee #2,**

192  
193 We would like to thank you for taking the time to review our manuscript. Your kind words about  
194 our work are greatly appreciated, and your comments have now been addressed and implemented  
195 in the revised manuscript. We have performed major revisions to accommodate your Comment  
196 #13, and we include the results in the revised version.  
197

198  
199 **Minor Comment #1:** P2, L38: ‘... together with the retrieval uncertainty of the SH products  
200 from all data sets, we conclude that RO observations are a valuable independent observing  
201 system.’ What do you mean by ‘independent’? RO SH is not independent from weather model  
202 data. JPL-RO SH makes use of the temperature from ECMWF. UCAR-RO SH is obtained by  
203 variational data assimilation utilizing ECMWF as the background. I suggest to remove the word  
204 ‘independent’. Also, ECMWF depends on RO, because UCAR-RO bending angles were  
205 assimilated.  
206

207 **Answer: Done.** We removed the word “independent”.  
208 -----  
209  
210

211 **Minor Comment #2:** P3, L48: ‘...Hence, we ought to quantify and understand the degree of  
212 agreement of water vapor concentration throughout the vertical extent of the troposphere among  
213 different sensors, in order to improve the representation of the Earth’s atmospheric humidity  
214 content that is key to predicting future climate [Hegerl et all., 2015].’ In the present study you  
215 consider the altitude range 700–400 hPa (~2–8 km). The troposphere extends from ~0–15 km. In  
216 fact, most of the water vapor is contained in the lowest 2 km. In the present study you do not try  
217 to quantify and understand the degree of agreement of the water vapor concentration throughout  
218 the vertical extent of the troposphere. I suggest to remove the word ‘throughout’.  
219

220 **Answer: Done.** We removed the word “throughout”. **Please, see strikethrough in line 49.**  
221 -----  
222  
223  
224

225 **Minor Comment #3:** P4, L83: ‘...and full diurnal cycle sampling.’ This is approximately true  
226 for COSMIC but not true in general. This depends on the LEO orbits.  
227

228 **Answer: Done.** We added the reviewer’s comment in the revised manuscript. **Please, see lines**  
229 **82–83.**  
230 -----

231 **Minor Comment #4:** P5, L102: ‘...Of importance is the fact that we use MERRA, instead of  
232 MERRA-2, because MERRA does not assimilate (unlike ERA-Interim), providing an  
233 independent data set when comparing the RO SH observations.’ This sounds interesting. Does  
234 this mean that you expect big differences when you use NERRA-2 instead of MERRA? Would it  
235 be a lot of effort for you to add MERRA-2 as well? I recommend to do so. This would be very  
236 interesting, because it would show the impact of RO on weather model SH.

237  
238 **Answer:** We believe that adding the MERRA-2 SH climatology in our analysis will not show  
239 the impact of RO on weather model SH. This is because there have been significant changes on  
240 how MERRA-2 handles the Earth’s water cycle with respect to MERRA, and these changes have  
241 a much more direct contribution to differences in MERRA-2 SH climatology than the addition of  
242 RO bending angles. Specifically, *Bosilovich et al. [2017]* state: “*Some of the changes in MERRA-2 have direct effect on the water cycle.*” For detailed explanation of these changes please refer to  
243 *Galero et al. [2016]* and *Takacs et al. [2016]*. Thus, we believe that comparisons with MERRA  
244 are more informative than comparisons with MERRA-2 for the objectives of our investigations,  
245 unless the contributions of all improvements in MERRA-2 are first isolated from the  
246 contributions of RO. However, we acknowledge the fact that comparing MERRA-2 and RO  
247 could be an interesting task. **We added relevant text to discuss this. Please, see lines 175–180.**

248  
249  
250  
251  
252 **Minor Comment #5:** P6, L114: ‘...We study the tropics and subtropics ( $\pm 40^\circ$ , three distinct  
253 latitudinal regions) from 700 hPa up to 400 hPa, because this region is key to climate research  
254 [IPCC, 2007], but models and observations have large SH differences in the middle and upper  
255 troposphere [e.g., Jiang et al., 2012; Tian et al., 2013; Wang and Su, 2013], and we select this  
256 pressure range because the RO SH retrievals are most robust.’ I can imagine what you mean by  
257 ‘most robust’ but some other interested readers do not know what this means. Please, explain in  
258 brief what you mean by ‘most robust’. E.g. signal tracking in the lower troposphere is somewhat  
259 problematic, the assumption of a spherically layered atmosphere, critical refraction (Ao et al.,  
260 2003) etc.

261  
262 **Answer:** We included relevant text and removed “most robust” to avoid confusion. **Please, see**  
263 **lines 121–127.**

264  
265  
266 **Minor Comment #6:** P7, L144: ‘...air temperature’. I suggest to remove the word ‘air’.

267  
268 **Answer: Done. Please, see strikethrough word in line 153.**

269  
270  
271  
272 **Minor Comment #7:** P7, L145: Please add (for completeness) the equation that you use to  
273 convert water vapor pressure to SH.

274  
275 **Answer: Done. Please, see lines 158–163.**

277 **Minor Comment #8:** P7, L154: ‘...air refractivity’. I suggest to remove the word “air” here and  
278 in the following.

279  
280 **Answer:** Done. Please, see ~~strikethrough~~ line 168.

281  
282  
283  
284  
285 **Minor Comment #9:** P9, L188: ‘...The AIRS physical retrievals use an IR-microwave neural net  
286 solution [Blackwell et al., 2008] as the first guess for temperature and water vapor profiles based  
287 on MIT’s stochastic cloud-clearing and neural network solution described in Khan et al. [2014].’  
288 I have very little idea of AIRS retrievals. In short, does the AIRS retrieval at any point make use  
289 of data from a climatology or a weather model?

290  
291 **Answer:** The short answer is no. The first guess comes from a neural network, which is trained  
292 on 60 days of ECMWF during the first year or two of AIRS operations [personal communication  
293 with Eric Fetzer]. It does not retrieve water profiles whenever cloud fraction exceeds the 80%,  
294 and recently they developed a cloud-clearing algorithm which compares the irradiance of  
295 neighboring pixels to infer the water vapor content during clouds.

296  
297  
298  
299  
300 **Minor Comment #10:** P9, L192: The section ‘Data Sources’ can be moved to the  
301 Acknowledgments.

302  
303 **Answer:** Done. Please, see Acknowledgments.

304  
305  
306  
307  
308 **Minor Comment #11:** P10, L207: ‘...GPS-RO air refractivity accuracy of <1.0% at 2.0 km  
309 altitude [Schreiner et al., 2007] reduces to ~0.2% above 5.0 km [Kuo et al., 2005].’ Schreiner et  
310 al., 2007 provides an estimate for the precision and not the accuracy. They measure the degree of  
311 the reproducibility of the GPS RO technique. Kuo et al., 2005 provide an estimate for the  
312 accuracy. As you focus on the altitude range 2 – 8 km, I suggest to simply write: ‘GPS-RO  
313 refractivity accuracy is about 1% at an altitude of 2 km and decreasing to about 0.2% at an  
314 altitude of 8 km [Kuo et al., 2005].’

315  
316 **Answer:** Done. Please, see lines 230–231.

321 **Minor Comment #12:** P10, L223: I suggest to remove ‘...We do not extend our analysis at  
322 higher altitudes due to small contribution of water vapor on to the RO observations.’ As you  
323 already mention in the ‘Methodology’ section that your focus is 700-400 hPa.  
324

325 **Answer: Done.** The sentence has been removed.  
326 -----  
327  
328  
329

330 **Minor Comment #13:** P11, L226: ‘...and the differences between the JPL and the UCAR time  
331 series serve as a guidline of an estimate of the SH structural uncertainty.’ One of the most  
332 interesting points in your study are the differences between JPL SH and UCAR SH. Where do  
333 the differences come from? Are those differences due to differences in the raw (=non-optimized)  
334 bending angles, the refractivity, or they mainly caused by the difference SH retrieval method? I  
335 strongly recommend to add (in an Appendix) a one-to-one comparison (mean and one-sigma) for  
336 bending angle and refractivity profiles for the altitude range 0-8 km.  
337

338 **Answer: Done.** This is similar to General Comment #3 of Reviewer #1. See new added Section  
339 **3.4.**  
340

341 The differences in the specific humidity retrievals result from a combination of different things.  
342 We have analyzed the refractivity climatologies from both JPL and UCAR at 700 hPa, 600 hPa,  
343 500 hPa, and 400 hPa pressure levels, and have included these results in the main manuscript.  
344 We also translate the refractivity differences into specific humidity differences and discuss the  
345 discrepancies between JPL and UCAR within these differences. We show these results for the  
346 deep tropics. The analysis is exactly the same for the trade winds zones and the subtropics and  
347 therefore we have not repeated it.  
348 -----  
349  
350

351 **Minor Comment #14:** P12, L240: ‘...SH time series over the entire observational record for all  
352 data sets throughout the vertical extent of the troposphere’. Remove the word ‘throughout’.  
353

354 **Answer: Done.** Please, see strikethrough in line 343.  
355 -----  
356  
357

358 **Minor Comment #15:** P18, L332: ‘...Overall, this suggests that over less convective regions  
359 different data sets tend to agree better, signifying that convection is a limiting factor in properly  
360 sensing the amount of water vapor in the atmosphere.’ Weather models are known to be less  
361 accurate in regions with convection. Do you mean that RO SH is less accurate there as well? For  
362 example there is one study by S. Yang and Zou, 2017 showing (positive) RO biases in cloudy  
363 conditions.  
364

365 **Answer: Done.** Please, see lines 526–528.  
366 -----

367 **Minor Comment #16:** P26, L421: Remove ‘in the forward operator’.

368

369 **Answer: Done.** Also removed in other places throughout the manuscript.

370 -----

371

372

373

374 **Comment #17:** P28, L467: I suggest to remove the word ‘independent’. RO (non-optimized)  
375 bending angles are independent, however RO SH is not independent.

376

377 **Answer: Done.** We replaced the word ‘independent’ with the word ‘additional’. **Please, see line**  
378 **530.**

379 -----

380

381

382

383

384

385

386

387

388

389

390

391

392

393

394

395

396

397

398

399

400

401

402

403

404

405

406

407

408

409

410

411

*Panagiotis Vergados*

412 **THIS IS THE END OF REVIEWER #2 REPORT .....**

413 **Comparisons of the tropospheric specific humidity from GPS radio occultations with**  
414 **ERA-Interim, NASA MERRA and AIRS data**

415

416 Panagiotis Vergados<sup>1</sup>, Anthony J. Mannucci<sup>1</sup>, Chi O. Ao<sup>1</sup>, Olga Verkhoglyadova<sup>1</sup>, and Byron  
417 Iijima<sup>1</sup>

418

419 <sup>1</sup> Jet Propulsion Laboratory, California Institute of Technology, Pasadena, California, USA

420

421 **Corresponding author:** P. Vergados, Jet Propulsion Laboratory, M/S 138-310B, 4800 Oak  
422 Grove Dr., Pasadena, CA, 91109, USA. (Panagiotis.Vergados@jpl.nasa.gov)

423

424

425

426

427

428

429

430

431

432

433 **Abstract.** We construct a 9-year data record (2007-2015) of the tropospheric specific humidity  
434 using Global Positioning System radio occultation (GPS RO) observations from the  
435 Constellation Observing System for Meteorology, Ionosphere, and Climate (COSMIC) mission.  
436 This record covers the  $\pm 40^\circ$  latitude belt and includes estimates of the zonally averaged monthly  
437 mean specific humidity from 700 hPa up to 400 hPa. It includes three major climate zones: a) the  
438 deep tropics ( $\pm 15^\circ$ ), b) the trade winds belts ( $\pm 15$ – $30^\circ$ ), and c) the subtropics ( $\pm 30$ – $40^\circ$ ). We find  
439 that the RO observations agree very well with the European Center for Medium-range Weather  
440 Forecasts Re-Analysis Interim (ERA-Interim), the Modern-Era Retrospective analysis for  
441 Research and Applications (MERRA), and the Atmospheric Infrared Sounder (AIRS) by  
442 capturing similar magnitudes and patterns of variability in the monthly zonal mean specific  
443 humidity and interannual anomaly over annual and interannual timescales. The JPL and UCAR  
444 specific humidity climatologies differ by less than 15% (depending on location and pressure  
445 level), primarily due to differences in the retrieved refractivity. In the middle-to-upper  
446 troposphere, in all climate zones, JPL is the wettest of all data sets, AIRS is the driest of all data  
447 sets, and UCAR, ERA-Interim, and MERRA are in very good agreement lying in between the  
448 JPL and AIRS climatologies. In the lower-to-middle troposphere, we present a complex behavior  
449 of discrepancies, and we speculate that this might be due convection and entrainment.  
450 Conclusively, the RO observations could potentially be used as a climate variable, but more  
451 thorough analysis is required to assess the structural uncertainty between centers and its origin.

**Comment [1]:**

Reviewer #1. General Comment #2.

Addressed and completed.

## 456 1 Introduction

457 The Intergovernmental Panel on Climate Change (IPCC) Fifth Assessment Report (AR5)

458 | [Flato *et al.*, 2013] reported that identifying the vertical structure of humidity is subject to great  
459 uncertainty, because dynamical processes that cannot be captured by one sensor alone drive  
460 water vapor. Hence, we ought to quantify and understand the degree of agreement of the water  
461 | vapor concentration ~~throughout the vertical extent of~~ in the troposphere among different sensors,  
462 in order to improve the representation of the Earth's atmospheric humidity content that is key to  
463 predicting future climate [Hegerl *et al.*, 2015].

## Comment [2]:

Reviewer #2. Minor Comment #2.

Addressed and completed.

464 To-date, ground- and space-based platforms, reanalyses, and model simulations do not  
465 provide precise knowledge of the water vapor's concentration, or its trends over time, in multiple  
466 regions of the Earth's atmosphere [Sherwood *et al.*, 2010]. This is because of a combination of  
467 different reasons that include: (a) sampling bias due to cloudiness, deep convection, or surface  
468 emissivity variations; (b) biases due to limited local time coverage, or random observations  
469 versus volume-filling scans; (c) coarse spatial resolution, and (d) misrepresentation of the  
470 planetary boundary layer's (PBL) moisture content [Hannay *et al.*, 2009] that induces errors in  
471 the lower-to-middle troposphere moist convection.472 In particular, infrared (IR) space-based platforms have a relatively coarse vertical  
473 resolution (e.g., 2.0–3.0 km), are prone to cloud contamination [Fetzer *et al.*, 2006], and tend to  
474 be biased low over wet and dry humidity extremes [Fetzer *et al.*, 2008; Chou *et al.*, 2009]. The  
475 use of IR observations in the lower troposphere still remains a challenge, due to the decreasing  
476 information content and the difficulty of detecting low-cloud contamination [Schreier *et al.*,  
477 2014]. Space-based microwave (MW) limb sounders, despite having low sensitivity to  
478 precipitation and clouds, have a coarse vertical resolution (e.g., 3.0 km in case of the Microwave

479 Limb Sounder (MLS) [Waters *et al.*, 2006] and are sensitive to the *a-priori* solution that could  
480 cause unsuccessful limb-viewing radiance retrievals (e.g., of up to 30% in the case of MLS  
481 [Read *et al.*, 2007]) under clear sky but moist conditions. Heavy cloudiness, especially in the  
482 middle-to-upper troposphere can also introduce biases in the upwelling MW radiation from water  
483 vapor due to the presence of ice particles that can contaminate the MW retrievals [Fetzer *et al.*,  
484 2008]. Global Circulation Models (GCMs) do not properly represent the middle troposphere  
485 moist convection [Sherwood *et al.*, 2004; Holloway and Neelin, 2009; Frenkel *et al.*, 2012], and  
486 large discrepancies in the tropospheric humidity among different reanalyses [Chen *et al.*, 2008]  
487 and among reanalyses, models, and satellite observations [Chuang *et al.*, 2010; Jiang *et al.*,  
488 2012; Tian *et al.*, 2013; Wang and Su, 2013] still persist.

489 The path towards constraining the models, reanalyses, and satellite water vapor  
490 observational uncertainties is to compare them against data sets that are as independent from  
491 their *a-priori* information as possible. Here, we use the multi-year observational record from  
492 Global Positioning System Radio Occultation (GPS RO) observations as such a data set, offering  
493 all-weather sensing, high vertical resolution (100–200 m; Kursinski *et al.* [2000]; Schmidt *et al.*  
494 [2005]), high specific humidity accuracy (< 1.0 g/Kg), and full diurnal cycle sampling (depending  
495 on the orbit and number of the RO spacecrafts).

496 Our primary objective is to create a short-term specific humidity data record (9 years)  
497 based on RO observations and compare it against NASA's Modern Era Retrospective Analysis  
498 for Research and Applications (MERRA), the European Center for Medium-range Weather  
499 Forecasts Reanalysis Interim (ERA-Interim), and Atmospheric Infrared Sounder (AIRS) data  
500 sets. Our goal is to evaluate the consistency of the RO specific humidity retrievals with respect to  
501 state-of-the-art reanalyses and satellite observations by quantifying the RO differences with the

**Comment [3]:**

Reviewer #2. Minor Comment #3.

**Addressed and completed.**

502 rest of the data sets over the tropics and subtropics. We anticipate gaining new insights about the  
503 specific humidity distribution over different convective regions, which could provide guidelines  
504 for future model improvements. The uniqueness of this investigation is that this is the first study  
505 to compare nearly a decade long data record of RO specific humidity information and their  
506 interannual variability against MERRA, ERA-Interim, and AIRS. [The description of the](#)  
507 [humidity retrieval process from RO observations is discussed in detail in Kursinski et al. \[1997\],](#)  
508 [Kursinski and Hajj \[2001\], and Collard and Healey \[2003\].](#) Of importance is the fact that we use  
509 MERRA, instead of MERRA-2, because MERRA does not assimilate ROs (unlike ERA-  
510 Interim), providing an independent data set when comparing the RO specific humidity  
511 observations.

512 Section 2 presents the data sets we use in this analysis together with their retrieval  
513 characteristics. In Section 3, we present and discuss the RO specific humidity climatologies with  
514 respect to the rest of the data sets and Section 4 summarizes our current research.

515

## 516 2 Methodology

517 We create time series of tropospheric specific humidity climatologies using the COSMIC  
518 observations (both the UCAR and the JPL retrievals), the MERRA and ERA-Interim data sets,  
519 and the Atmospheric Infrared Sounder (AIRS) observations. These climatologies contain a 9-  
520 year measurement record from January 2007 until December 2015 and represent monthly zonal  
521 mean averages. We study the [geographic region between  \$\pm 40^\circ\$  latitude, which we divide into](#)  
522 [three distinct dynamical regions: a\) the deep tropics \( \$\pm 15^\circ\$ \), b\) the middle tropics \( \$\pm 15^\circ\$ – \$30^\circ\$ \), and](#)  
523 [c\) the subtropics \( \$\pm 30^\circ\$ – \$40^\circ\$ \).](#) In each region, we study the annual and interannual variability and  
524 [trend of the specific humidity from all data sets, and then we quantify the mean differences and](#)

525 standard deviations of all climatologies with respect to the JPL climatology (that we use as a  
526 reference). The time series represent monthly zonal averages of the specific humidity at  
527 individual pressure levels from the lower to the middle troposphere: 700 hPa, 600 hPa, 500 hPa,  
528 and 400 hPa.

529 We are particularly interested in investigating the performance of the RO specific  
530 humidity climatologies with respect to other databases within  $\pm 40^{\circ}$  latitude, as it is a key region  
531 for climate research [IPCC, 2007], and because models and observations exhibit large  
532 differences in the middle and upper troposphere in this band [e.g., Jiang *et al.*, 2012; Tian *et al.*,  
533 2013; Wang and Su, 2013]. We focus between 700 hPa and 400 hPa, because although tracking  
534 of the GPS signals in the lower troposphere (e.g., below 700 hPa) has been greatly improved  
535 with the use of open loop tracking techniques [Sokolovskiy *et al.*, 2006], the presence of the  
536 water vapor and small signal-to-noise ratio could still cause loss of lock for lower altitudes.  
537 Additionally, atmospheric ducting at and below the planetary boundary layer could also lead to  
538 negative refractivity biases [Ao *et al.*, 2003; Xie *et al.*, 2010]. Above 400 hPa, the signature of  
539 water vapor on the atmospheric refractivity is small, leading to larger retrieval errors.

540

## 541 2.1 Constellation Observing System for Meteorology, Ionosphere and Climate

542 The COSMIC constellation of six microsatellites were launched in April 2006 orbiting  
543 the Earth at an altitude of  $\sim 800$  km in near-circular Low Earth Orbit (LEO) [Anthes *et al.*, 2008].  
544 They measure the phase and amplitude of the transmitted dual frequency *L*-band GPS signals  
545 ( $f_1=1.57542$  GHz;  $f_2=1.22760$  GHz) as a function of time. The relative motion of the COSMIC  
546 satellites with respect to the GPS satellites and the presence of the atmosphere cause a Doppler  
547 frequency shift on the transmitted GPS signals received by the COSMIC satellites. The

**Comment [4]:**

Reviewer #1. Specific Comment #4.

Reviewer #2. Minor Comment #5.

**Addressed and completed.**

548 magnitude of the Doppler frequency shift is estimated as the time derivative of the recorded GPS  
549 signal phases, which together with precise knowledge of the position and velocity information of  
550 both the COSMIC and the GPS satellites allows for estimation of the amount of bending of the  
551 transmitted GPS signals due to the presence of the atmosphere, from which one can infer the air  
552 refractive index [Kursinski *et al.*, 1997]. In the lower troposphere, the bending angle is retrieved  
553 using radioholographic methods (such as canonical transform or full spectrum inversion) that  
554 eliminate errors due to atmospheric multipath [e.g., Ao *et al.*, 2003]. The relative motion of the  
555 COSMIC and GPS satellite pair allows for the vertical scanning of the atmosphere providing  
556 vertical profiles of atmospheric refractivity, which contain temperature and humidity  
557 information.

558 We use RO-derived specific humidity products from both the UCAR and the JPL  
559 processing centers, which follow different processing techniques. Although this study does not  
560 focus on these differences, we note that UCAR adopts a variational assimilation method, which  
561 requires *a-priori* estimates of the atmospheric water vapor content (provided by ERA-Interim),  
562 implying that the derived specific humidity products may be subject to the error characteristics of  
563 the humidity initialization. On the other hand, JPL uses the refractivity equation (along with the  
564 hydrostatic equation and equation of state) to estimate the water vapor pressure given *a-priori*  
565 knowledge of air temperature [Hajj *et al.*, 2002]:

566

$$N = 77.6 \frac{P}{T} + 3.73 \cdot 10^5 \frac{e}{T^2} \Leftrightarrow e = \frac{1}{3.73 \cdot 10^5} (NT^2 - 77.6PT) \quad [1]$$

567

568 Where  $N$  (unitless) is the refractivity,  $P$  (mbar) is the pressure,  $T$  (K) is the temperature, and  $e$   
569 (mbar) is the RO-derived water vapor pressure. [The equation we use to convert the water vapor](#)

**Comment [5]:**

Reviewer #2. Minor Comment #6.

Addressed and completed.

**Comment [6]:**

Reviewer #1. General Comment #2.

Addressed and completed.

570 pressure into specific humidity is given by:

571

$$q = 621.9907 \cdot \frac{e}{(P - e)} \quad [2]$$

572

573 Where  $q$  (g kg<sup>-1</sup>) is the specific humidity,  $P$  (mbar) is the pressure, and  $e$  (mbar) is the RO-

574 derived water vapor pressure. The retrieval errors of the JPL SH products do not contain *a-priori*

575 humidity information, but are subject to errors in the *a-priori* temperature information, which is

576 provided by the ECMWF Tropical Ocean and Global Atmosphere (TOGA) database. Because

577 Eq. (1) requires that both the RO and the ECMWF TOGA data sets be reported at the same

578 pressure levels, we interpolate the temperature profiles into the vertical grid of the RO profiles

579 using linear interpolation in the log pressure domain. Currently, the JPL-retrieved COSMIC 

580 refractivity profiles are provided at 200 m vertical resolution in the lower to middle troposphere.

581

## 582 2.2 Modern-Era Retrospective Analysis for Research and Application

583 We use the MERRA (v5.2.0) analysis that employs a 3-D variational assimilation

584 technique based on the Gridpoint Statistical Interpolation (GIS) scheme with a 6-hour update

585 cycle [e.g., Wu *et al.*, 2002]. It did not yet assimilate RO observations, and therefore, it is an

586 independent dataset from COSMIC. Besides MERRA-2 assimilating GPS RO bending angle

587 observations, it also includes significant changes with respect to MERRA in regards to moisture

588 analysis that have a direct affect on the water cycle [Gelaro *et al.*, 2016; Takacs *et al.*, 2016;

589 Bosilovich *et al.*, 2017]. Although GPS RO comparisons with MERRA-2 could provide valuable

590 statistics, they would not represent a clear picture of the effect of assimilating GPS RO

591 observations, unless the impact of all other improvements on the humidity climatology is first

**Comment [7]:**

Reviewer #2. Minor Comment #7.

**Addressed and completed.**

**Comment [8]:**

Reviewer #1. Specific Comment #6.

**Addressed and completed.**

**Comment [9]:**

Reviewer #2. Minor Comment #8.

**Addressed and completed.**

592 | **determined.** We analyze the monthly gridded specific humidity products given in a 1/2-degree x  
593 | 2/3-degree latitude-longitude grid and 42 vertical pressure levels. In the troposphere, the vertical  
594 | pressure resolution from the surface up to 700 hPa is 25 hPa, whereas from 700 hPa until 300  
595 | hPa the vertical resolution is 50 hPa. MERRA is a NASA analysis that assimilates satellite  
596 | observations using Goddard's Earth Observing System (GOES) version 5.2.0 Data Assimilation  
597 | System (DAS) [Rienecker *et al.*, 2008]. Primarily, it assimilates radiances from AIRS, the  
598 | Advanced Television and Infrared Observatory Spacecraft Operational Vertical Sounder  
599 | (ATOVS), and the Special Sensor Microwave Imager (SSM/I), and figure 4 in Rienecker *et al.*  
600 | [2011] provides a detailed list of the rest of the data sets that are assimilated.

601

### 602 | **2.3. European Center for Medium-Range Weather Forecasts Re-Analysis Interim**

603 | We use the ERA-Interim [Dee *et al.*, 2011], which uses a 4-D variational assimilation  
604 | technique [Simmons *et al.*, 2005] to analyze a variety of observational data sets to predict the  
605 | state of the atmosphere with accuracy similar to what is theoretically possible based on the error  
606 | characteristics of the assimilated data [Simmons and Hollingsworth, 2002]. We analyze the  
607 | monthly gridded SH products given in a 0.75 degree x 0.75 degree latitude-longitude grid and 20  
608 | pressure levels from 1000 hPa up to 300 hPa. The vertical resolution from the surface up to 750  
609 | hPa is 25 hPa, but the vertical resolution decreases to 50 hPa between 750 hPa and 300 hPa. The  
610 | primary data sets assimilated in ERA-Interim are radiosonde humidity observations, AIRS and  
611 | microwave radiances, and as of November 2006, the GPS RO bending angle profiles.

612

### 613 | **2.4. Atmospheric Infrared Sounder**

614 | We use the AIRS/AMSU v6 Level-3 data [Tian *et al.*, 2013a] and analyze the monthly

**Comment [10]:**

Reviewer #2. Minor Comment #4.

**Addressed and completed.**

615 gridded SH product given in a 1-degree x 1-degree latitude-longitude grid, which extend from  
616 the surface up to 100 hPa in 12 vertical pressure levels ( $\sim 2.0$  km vertical resolution). The latest  
617 AIRS v6 SH products are now available at standard pressure levels. The vertical resolution  
618 between the surface up to 850 hPa is 75 hPa; between 700 hPa and 300 hPa the vertical  
619 resolution decreases to 100 hPa, and above the 300 hPa pressure level up to 100 hPa the vertical  
620 resolution is 50 hPa. The AIRS physical retrievals use an IR–microwave neural net solution  
621 [Blackwell *et al.*, 2008] as the first guess for temperature and water vapor profiles based on  
622 MIT's stochastic cloud-clearing and neural network solution described in Khan *et al.* [2014].

623

## 624 **2.5. Establishing Data Set Accuracy**

625 *Kursinski et al.* [1995] estimated that occultation water vapor pressure profiles at the  
626 tropics have a precision between 10 and 20% below 7.0 km altitude assuming temperature errors  
627 of 1.5 K, surface pressure errors of 3 mbar, and refractivity errors of < 0.2%, which translate to a  
628 specific humidity precision of < 0.25 g kg<sup>-1</sup> at 700 hPa and < 0.03 g kg<sup>-1</sup> at 400 hPa, given a  
629 mean specific humidity of 4.0 g kg<sup>-1</sup> at 700 hPa and 1.0 g kg<sup>-1</sup> at 400 hPa between 01/2007 and  
630 21/2015. *Kursinski and Hajj* [2001] determined that the precision of individual occultation  
631 specific humidity profiles is ~0.20–0.50 g kg<sup>-1</sup> in the middle-to-lower troposphere. *Ho et al.*  
632 [2007] combined AIRS and RO data retrieving specific humidity profiles in the lower  
633 troposphere with root-mean-square-error (RMSE) between 0.40 g kg<sup>-1</sup> (at 700 hPa) and 0.05 g  
634 kg<sup>-1</sup> (at 400 hPa). *Ho et al.*, [2010] collocated RO and ECMWF profiles near radiosonde  
635 locations and estimated that the standard deviation of the differences between the two data sets is  
636 < 0.50 g kg<sup>-1</sup> above 3.0 km altitude. *Kishore et al.*, [2011] estimated that the differences between  
637 the ERA-Interim and COSMIC are -0.15±0.22 g kg<sup>-1</sup> at 3.0 km and -0.07±0.06 g kg<sup>-1</sup> at 7.0 km,

638 in the deep tropics ( $\pm 20^\circ$ ). They also estimated that the differences between the Japanese Re-  
639 Analysis 25-year (JRA-25) and COSMIC are about  $-0.10 \pm 0.23 \text{ g kg}^{-1}$  at 3.0 km and  $-0.20 \pm 0.06 \text{ g}$   
640  $\text{kg}^{-1}$  at 7.0 km. *Ao et al.* [2012] estimated that the specific humidity precision is  $\sim 0.15 \text{ g kg}^{-1}$  per  
641 degree kelvin error in temperature. *Vergados et al.* [2014] reported that RO specific humidity is  
642 retrieved within  $\sim 0.20\text{--}0.40 \text{ g kg}^{-1}$  accuracy at the tropics, provided the RO refractivity accuracy  
643 is  $\sim 1.0\%$  at an altitude of 2.0 km decreasing to  $\sim 0.2\%$  at an altitude of 8.0 km [Kuo et al., 2005]  
644 and a temperature error of  $\pm 1.0 \text{ K}$ . Recently, *Kursinski and Gebhardt* [2014] proposed a novel  
645 approach to further improve the retrieved humidity accuracy and precision from RO observations  
646 in the middle troposphere.

Comment [11]:

Reviewer #2. Minor Comment #11.

Addressed and completed.

647 Conclusively, the specific humidity accuracy and precision from RO observations  
648 depends on altitude and we determine it to be  $\sim 10\text{--}20\%$ . MERRA assimilates various  
649 observational data sets and the SH accuracy is a function of the accuracy of the assimilated  
650 products. In general, the MERRA specific humidity retrievals are accurate to  $\sim 20\%$  [Rienecker et  
651 al., 2011]. AIRS estimated specific humidity product accuracies are typically  $\sim 25\%$  at  $p > 200$   
652 hPa [Fetzer et al., 2008], and ERA-Interim specific humidity products have an estimated  
653 accuracy of  $\sim 7\text{--}20\%$  in the tropical lower-to-middle troposphere [Dee et al., 2011]. The RO  
654 retrievals seem to have better accuracy than the AIRS retrievals, which could be attributed to the  
655 fact that the RO observations are based on precise time measurements and have very low  
656 sensitivity to clouds (unlike the IR observations). In general, the RO observations seem to have  
657 similar accuracy and precision with both the MERRA and ERA-Interim reanalyses.

Comment [12]:

Reviewer #1. General Comment #3.

Addressed and completed.

### 659 3. Results and Discussion

#### 660 3.1. Analysis of the specific humidity in the deep tropics

Comment [13]:

Reviewer #1. Specific Comment #3.

Addressed and completed.

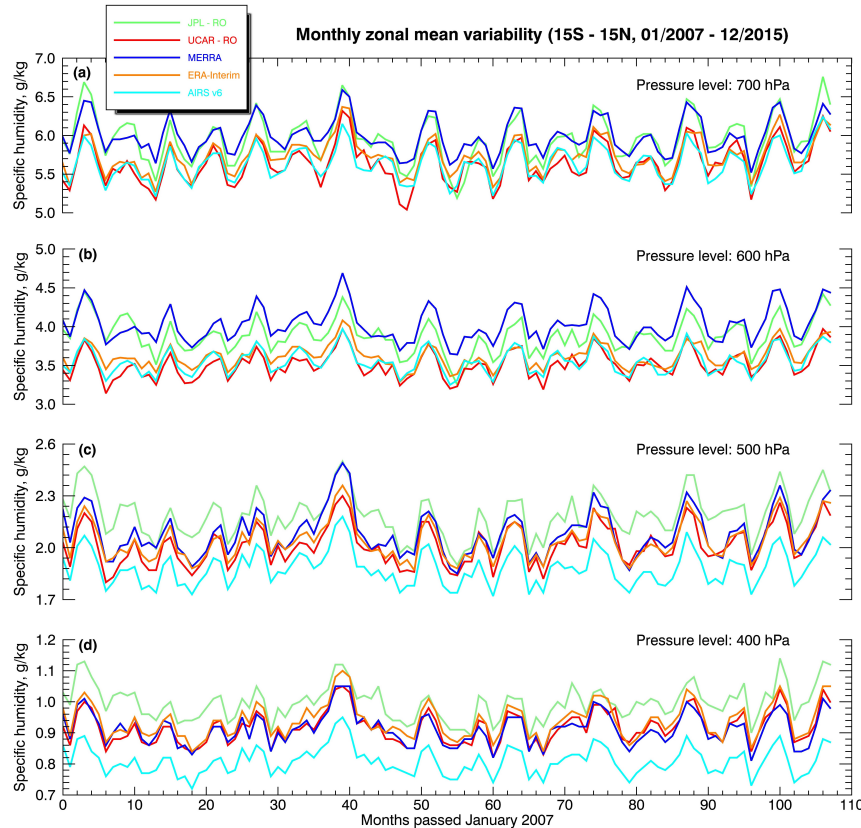
Comment [14]:

Note: We deleted this text, because we have already mentioned this details in the Methodology Section.

Deleted: We divide this section into three sub sections that represent the three tropical climate environments we analyse, each of which exhibits different atmospheric dynamic properties. In each sub section, we study the long term SH in terms of (a) annual and interannual variability and trend, and (b) deviations with respect to our center's SH values (P1-RO). The time series represent monthly zonal averages of the SH at individual pressure levels from the lower up to the middle troposphere: 700 hPa, 600 hPa, 500 hPa, and 400 hPa. We do not extend our analysis to higher altitudes due to the small contribution of water vapor on to the RO observations.

676 The latitude belt within  $\pm 15^\circ$  encompasses the ascending branch of the Hadley cell  
 677 circulation. Near to the surface, moist air masses from both hemispheres converge within this  
 678 narrow equatorial region, collide, and lead to heavy precipitation. The amount of the latent heat  
 679 released during rainfall warms the air driving strong rising motions, deep convection, and high  
 680 cloud formation.

681



682

683 **Figure 1.** Times series of the monthly zonal averages of the specific humidity from January 1,  
 684 2007 until December 31, 2015 from JPL (green), UCAR (red), ERA-Interim (orange), MERRA  
 685 (blue) and AIRS (cyan) at (a) 500 hPa, (b) 400 hPa, (c) 700 hPa, and (d) 600 hPa pressure levels.

686 Figure 1 shows the [monthly zonal mean specific humidity](#) as a function of time from  
 687 [January 2007 until December 2015](#) from 700 hPa up to 400 hPa. Qualitatively, all [data sets](#)  
 688 capture the same variability pattern, exhibiting clear signatures of an annual and interannual  
 689 cycle at all pressure levels. [Quantitatively, the magnitude of the specific humidity varies among](#)  
 690 [data sets having a minimum value of 5.0 g kg<sup>-1</sup>](#) (summer and winter) and a maximum value of  
 691 [6.5 g kg<sup>-1</sup>](#) (spring and autumn) at 700 hPa. Its value decreases with altitude and at 400 hPa  
 692 [fluctuates between 0.7 g kg<sup>-1</sup>](#) (during summer and winter) and 1.0 g kg<sup>-1</sup> (during spring and  
 693 [autumn\). Table 1 shows that the 9-year mean differences among all climatologies are < 20%,](#)  
 694 [falling within the level of retrieval uncertainty of individual RO specific humidity profiles.](#)

695

696 **Table 1.** Mean climatology, deviation of the mean climatology from JPL, and linear regression  
 697 fits of the specific humidity time series from JPL, UCAR, ERA-Interim, MERRA, and AIRS  
 698 over the  $\pm 15^\circ$  climate region. The 2-sigma uncertainties are estimated for each statistical metric,  
 699 and their statistical significance is evaluated at  $p < 0.05$  confidence level. Boxes filled with red  
 700 are statistically insignificant.

**PART I: 9-year long mean of specific humidity climatology with 2-sigma uncertainty, g kg<sup>-1</sup>**

Data Records	JPL	UCAR	ERA-Interim	MERRA	AIRS
400 hPa	$0.99 \pm 0.12$	$0.92 \pm 0.10$	$0.94 \pm 0.12$	$0.91 \pm 0.10$	$0.81 \pm 0.08$
500 hPa	$2.18 \pm 0.26$	$2.01 \pm 0.22$	$2.04 \pm 0.22$	$2.08 \pm 0.26$	$1.88 \pm 0.20$
600 hPa	$3.88 \pm 0.44$	$3.51 \pm 0.30$	$3.62 \pm 0.30$	$4.03 \pm 0.44$	$3.55 \pm 0.32$
700 hPa	$5.95 \pm 0.60$	$5.64 \pm 0.52$	$5.74 \pm 0.46$	$5.99 \pm 0.46$	$5.64 \pm 0.44$

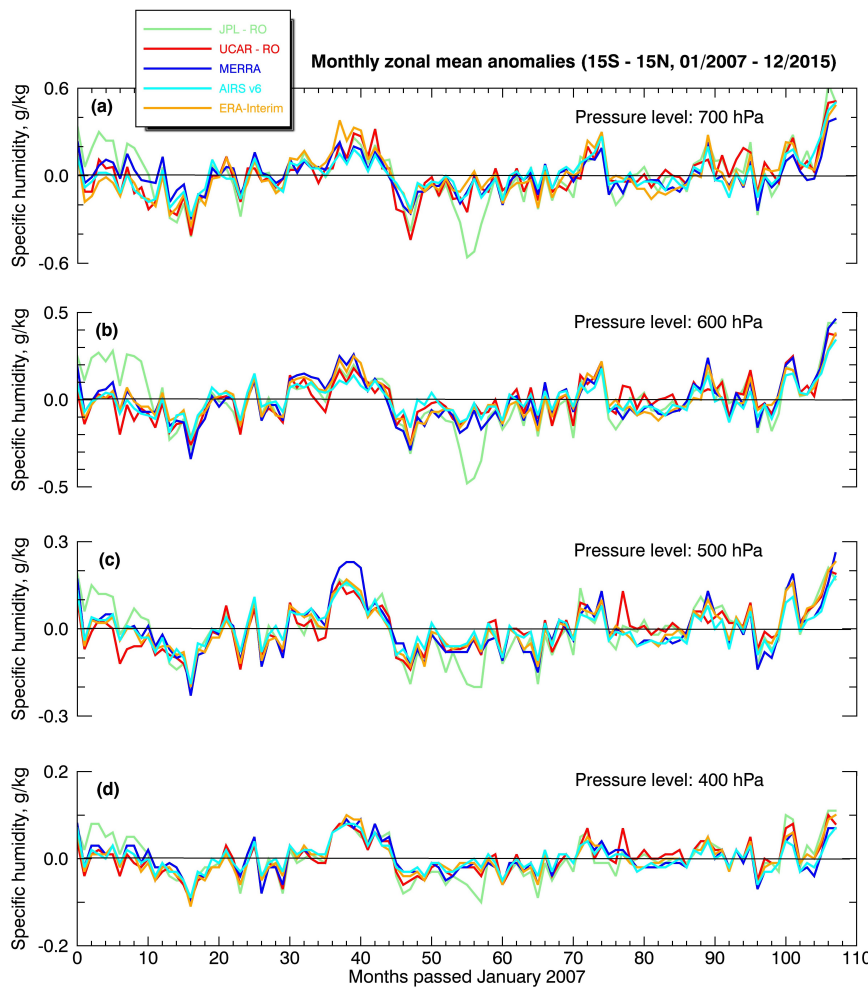
**PART II: 9-year long mean of specific humidity deviations from JPL-RO, g kg<sup>-1</sup>**

400 hPa	n/a	- 0.08	- 0.06	- 0.08	- 0.19
500 hPa	n/a	- 0.17	- 0.14	- 0.10	- 0.31
600 hPa	n/a	- 0.37	- 0.27	+ 0.15	- 0.33
700 hPa	n/a	- 0.31	- 0.22	+ 0.04	- 0.32

**PART III: Linear regression of specific humidity anomalies with 2-sigma uncertainty, g kg<sup>-1</sup> month<sup>-1</sup>**

400 hPa	$(1.0 \pm 3.0) \times 10^{-4}$	$(3.7 \pm 2.2) \times 10^{-4}$	$(2.4 \pm 2.2) \times 10^{-4}$	$(0.1 \pm 2.1) \times 10^{-4}$	$(0.3 \pm 2.0) \times 10^{-4}$
500 hPa	$(2.3 \pm 6.0) \times 10^{-4}$	$(9.6 \pm 4.4) \times 10^{-4}$	$(6.2 \pm 4.6) \times 10^{-4}$	$(3.3 \pm 5.4) \times 10^{-4}$	$(2.1 \pm 4.2) \times 10^{-4}$
600 hPa	$(-1.8 \pm 10) \times 10^{-4}$	$(15.1 \pm 6.6) \times 10^{-4}$	$(6.3 \pm 6.8) \times 10^{-4}$	$(8.4 \pm 8.0) \times 10^{-4}$	$(6.3 \pm 5.4) \times 10^{-4}$
700 hPa	$(6.1 \pm 12) \times 10^{-4}$	$(17.2 \pm 9.0) \times 10^{-4}$	$(14.1 \pm 8.8) \times 10^{-4}$	$(1.3 \pm 7.2) \times 10^{-4}$	$(12.9 \pm 7.2) \times 10^{-4}$

701 Due to averaging over 9 years, random and systematic errors in the time series are  
 702 significantly reduced, representing the degree of disagreement among climatologies. Despite  
 703 these differences, figure 2 shows that all interannual anomaly climatologies not only capture the  
 704 same variability patterns but they also have almost similar magnitudes. Their amplitude  
 705 fluctuates around  $\pm 0.4 \text{ g kg}^{-1}$  at 700 hPa and decreases with altitude to  $\pm 0.1 \text{ g kg}^{-1}$  at 400 hPa.



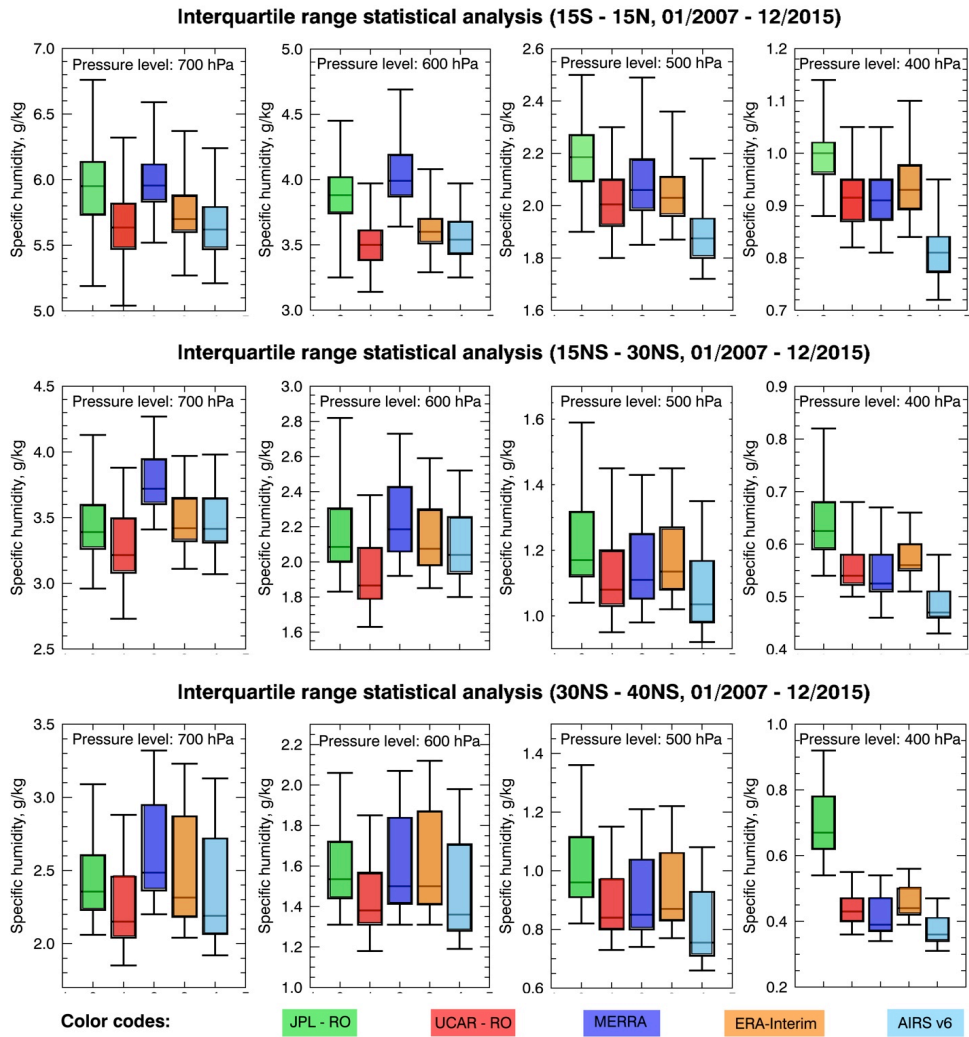
706  
 707 **Figure 2.** This is the same as figure 1, but for the specific humidity interannual anomalies.

708 During the strong La Niña event in 2010–2011 all interannual anomaly climatologies  
709 captured an enhancement in specific humidity with respect to the background, which is more  
710 pronounced at 500 hPa and 400 hPa marking the highest values in the time series. An even  
711 stronger El Niño event occurred in 2015–2016 and the interannual anomalies in all climatologies  
712 also started showing a pronounced increase in specific humidity. Interestingly, during the strong  
713 La Niña event in 2007–2008, only the JPL climatology displayed increased specific humidity  
714 values compared to the rest of the rest climatologies. The interannual anomaly variations for all  
715 data sets in the middle troposphere correlate strongly ( $> 0.8$ ) with those in the lower troposphere,  
716 but have smaller amplitude.

717 A linear regression fit and a Student *t*-test on the specific humidity interannual anomalies  
718 shows that the JPL and MERRA series do not suggest an increase in specific humidity with time  
719 between 700 hPa and 400 hPa (cf., Table 1). However, the UCAR and ERA-Interim data sets  
720 show an increase of the tropospheric specific humidity, with slower increase rate with increasing  
721 altitude. The difference between the two data sets is that UCAR-RO suggests faster moistening  
722 of the troposphere than ERA-Interim. The AIRS data sets also show an increase of the specific  
723 humidity at 700 hPa and 600 hPa at a rate similar to that of ERA-Interim, but no SH increase at  
724 500 hPa and above.

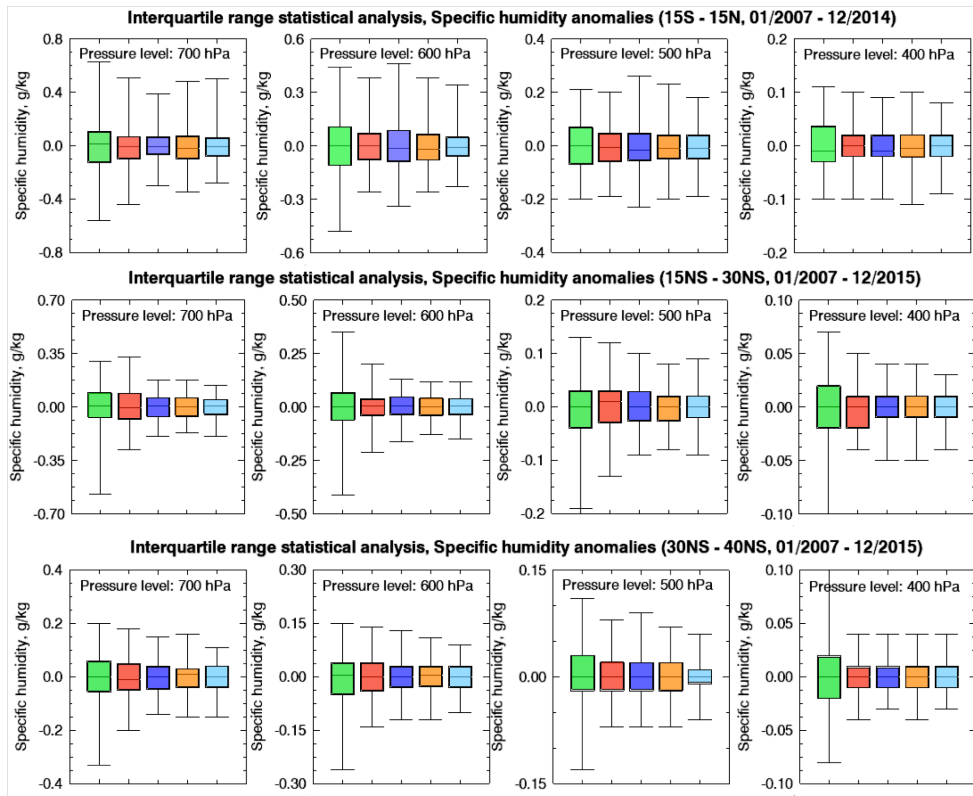
**Deleted:** we find  
**Deleted:** suggest  
**Deleted:** the amount of SH  
**Deleted:** Contrary to that,  
**Deleted:** indicate a gradual increase of the absolute amount of SH throughout the vertical extend of the troposphere  
**Deleted:** . The increase is faster at 700 hPa and slows down  
**Deleted:** height  
**Deleted:** with  
**Deleted:** systematically indicating  
**Deleted:** SH

725 We statistically analyze the 9-year time series of the absolute specific humidity (cf.,  
726 figure 1) and interannual anomaly climatologies (cf., figure 2) by estimating their respective  
727 interquartile ranges as shown in figures 3 and 4. In these box plots, the solid black line inside the  
728 boxes represents the median value of the 9-year climatologies. The length of the box represents  
729 the value range within which we find 50% of the values around the median. The top and bottom  
730 whiskers define the largest and the lowest monthly zonal mean values of the time series.



744

745 | **Figure 3.** Boxplots of the monthly zonal mean specific humidity throughout the 2007–2015 time  
 746 | period for the 700 hPa, 600 hPa, 500 hPa, and 400 hPa over the ascending branch of Hadley cell  
 747 | ( $\pm 15^\circ$ ) (top row), the trade winds belt ( $\pm 15$ – $30^\circ$ NS) (middle), and the descending branch of  
 748 | Hadley cell at the subtropics ( $\pm 30$ – $40^\circ$ ) from JPL (green), UCAR (red), MERRA (blue), ERA–  
 749 | Interim (orange), and AIRS (cyan).



750 **Figure 4.** This is the same as figure 3, but for the specific humidity interannual anomalies.

751  
 752  
 753 The top row in figure 1 presents statistical information about the median, the interquartile range  
 754 (IQR), and the minimum and maximum values of the specific humidity time series over the  
 755 entire observational record for all data sets throughout the vertical extent of the troposphere.  
 756 Figure 2 shows details about the variability of the monthly zonal mean SH and Table 1  
 757 summarizes the results of figure 2.

758 Figure 3 shows that in the lower troposphere, above the planetary boundary layer, the JPL  
 759 and MERRA products show almost the same median value of  $\sim 6.0 \text{ g kg}^{-1}$  (at 700 hPa) and  $\sim 4.0 \text{ g}$

Comment [15]:

Reviewer #2. Minor Comment #14.

Addressed and completed.

760  $\text{kg}^{-1}$  (at 600 hPa). Their difference is  $< 1.0\%$  and  $< 4.0\%$  at 700 hPa and 600 hPa, respectively  
761 (cf., Table 1) marking their excellent agreement. The UCAR, AIRS, and ERA-Interim data sets  
762 are in a very good agreement with one another differing by  $< 3.0\%$ , and they are drier than the  
763 JPL and MERRA products by  $\sim 7.0\text{--}10\%$ . This dryness is more pronounced at 600 hPa. In the  
764 middle troposphere, at 500 hPa and 400 hPa, the MERRA, ERA-Interim, and UCAR  
765 climatologies start agreeing very well with each other capturing  $2.0 \text{ g kg}^{-1}$  at 500 hPa and  $0.9 \text{ g}$   
766  $\text{kg}^{-1}$  at 400 hPa. JPL appears to be the moistest of all data sets by  $< 10\%$ , whereas AIRS is the  
767 driest of all data sets by  $\sim 15\text{--}25\%$  and its dryness is more apparent at 400 hPa.

768 Figure 4 summarizes the statistics of all specific humidity interannual anomaly  
769 climatologies. Despite the differences in the absolute values, the interannual anomalies: a) have  
770 almost the same median value, b) have similar IQRs, and c) exhibit similar scattering around the  
771 median with almost the same maximum and minimum values. This behavior is seen at 700 hPa  
772 up to 400 hPa, with the scattering around the median to be more consistent among the  
773 climatologies at higher altitudes. We should point out that the pronounced AIRS dry bias over  
774 the deep tropics ITCZ [Hearty *et al.* 2014], due to sampling limitations over cloud-covered  
775 regions, can explain the observed systematic lower specific humidity values with respect to all  
776 data sets from 700 hPa up to 400 hPa. This suggests that IR observations over deep convective  
777 environments do not properly capture the amount of water vapor in the atmosphere.

778 ~~ERA-Interim underestimates the total cloud fraction over the  $\pm 15^\circ$  region compared to~~  
779 ~~MERRA [Dolinar *et al.*, 2016; figure 1]~~ and is also colder than MERRA by  $1.0 \text{ K}$  in the 2006  
780 ~~2011 time period at the tropics at 700 hPa [Simmons *et al.*, 2014; figure 18]~~. Given the definition  
781 ~~of specific humidity (as the product between the relative humidity and the saturation vapor~~  
782 ~~pressure), it is evident why MERRA shows a wetter air than ERA-Interim in the lower~~

783 troposphere. However, the cold bias in the ERA Interim becomes small with altitude and  
784 reduces to almost zero at 500 hPa, and ERA Interim starts showing a warm bias with respect to  
785 MERRA at 300 hPa by  $-0.1\text{--}0.3$  K [Simmons *et al.*, 2014]. This temperature bias between the  
786 two reanalyses could possibly explain why the two reanalyses begin to estimate similar SH  
787 values at 500 hPa and 400 hPa.

788

### 789 3.2. Analysis of the specific humidity at the trade winds zones

790 The  $\pm 15\text{--}30^\circ$  latitudinal belt, in both hemispheres, defines the trade winds zones, where  
791 dry air masses descending from the Hadley cell at the subtropics travel towards the equator.  
792 These regions exhibit shallower convection compared to the deep tropics, as clouds forming in  
793 these regions are typically cumulus and do not extend above 4.0 km.

794 Figures S1 and S2 (cf., supplementary material) show that the specific humidity  
795 climatology and the respective interannual anomaly for all data sets capture distinct annual and  
796 interannual variability patterns at all pressure levels. The specific humidity is lower in the trade  
797 winds zone than in the deep tropics ranging from  $2.5\text{--}4.5$  g kg $^{-1}$  at 700 hPa to  $0.45\text{--}0.75$  g kg $^{-1}$  at  
798 400 hPa and the amplitude of the interannual anomalies is  $\sim 50\%$  smaller in the 700–400 hPa  
799 pressure range. The interannual anomalies are also correlated between 700 hPa and 400 hPa ( $>$   
800 0.6), but their degree of correlation is weaker than that over the deep tropics, and we do not  
801 observe enhanced values during the strong La Niña and El Niño events as we observe over the  
802 deep tropics. We suggest that this may be due to weaker convection over the trade winds zone  
803 compared to the deep tropics; thus, establishing a weaker vertical connection. In the trade winds  
804 zone, all data sets do not suggest a statistically significant increase in specific humidity (cf.,  
805 Table S1), but we ought to point out that the linear regression fit slopes are negative.

**Comment [16]:**

**Note:** We decided to remove this detail, because this manuscript does not focus on the differences between the re-analyses.

806 Table S1 shows that the mean differences of the specific humidity over the 9-year period,  
807 between JPL and the rest of the data sets, is smaller at 700 hPa, 600 hPa, and 500 hPa than the  
808 differences in the deep tropics, except at 400 hPa where it remains almost the same. These  
809 differences are smaller than 20% and fall within the retrieval uncertainty of the data sets. It  
810 appears that over less convective regions the climatologies agree better with one another  
811 suggesting that convection could be a limiting factor in properly sensing the amount of  
812 water vapor in the atmosphere.

813 Figure 3 (middle row) and figure S1 show that the specific humidity climatologies in the  
814 trade winds zone have similar characteristics with the deep tropics at 500 hPa and 400 hPa. The  
815 JPL data set appears to be again the wettest and the AIRS the driest compared to all  
816 climatologies, whereas UCAR, ERA-Interim, and MERRA show a very good agreement in  
817 between. The reason JPL appears to be the wettest at 500 hPa is because the summer season in  
818 all years is wetter by ~4.0% than the rest of the data sets, but this difference is within the  
819 systematic uncertainty of the retrievals. However, at 700 hPa and 600 hPa, we notice a different  
820 behavior in terms of the data sets' agreement compared to our analysis in the deep tropics.  
821 Specifically, the JPL, ERA-Interim, and AIRS data sets agree very well with one another having  
822 differences of ~ 1.0% (at 700 hPa) and ~ 2.0–3.0% (at 600 hPa); but, these differences are  
823 statistically insignificant. UCAR is the driest of all data sets by ~15% (with respect to MERRA)  
824 and ~ 5.0–10% (with respect to JPL), and MERRA seems to overestimate the specific humidity  
825 particularly at 700 hPa.

826 Figure 4 (middle row) and figure S2 show that the specific humidity interannual  
827 anomalies are in excellent agreement with one another having almost the same median value,  
828 similar IQR, and exhibit similar scattering around the median. The exception is the JPL

829 climatology, which shows larger scattering towards negative anomaly values. This could be due  
830 to outliers in the data, which push down the lowest negative value. This behavior is seen at 700  
831 hPa up to 400 hPa and unlike the deep tropics, we do not observe enhanced specific humidity  
832 anomaly values in the climatologies during the strong La Niña and El Niño events (Figure S2).

833

834 **3.3. Analysis of the specific humidity at the subtropics**

835 The  $\pm 30\text{--}40^\circ$  latitude belt, in both hemispheres, defines the subtropics where dry air  
836 descends from the Hadley cell. These moderate-to-strong subsidence regions exhibit low cloud  
837 formation (especially during the summer months), while favoring formation of low-altitude  
838 marine boundary layer (MBL) clouds.

**Comment [17]:**

Reviewer #1. Specific Comment #8.

Addressed and completed.

839 Figures S3 and S4 (cf., supplementary material) show that the specific humidity  
840 climatology shows a distinct annual cycle signature at all pressure levels, with lower values  
841  $\sim 2.0\text{--}3.5 \text{ g kg}^{-1}$  at 700 hPa to  $0.3\text{--}0.6 \text{ g kg}^{-1}$  at 400 hPa (except for the JPL climatology that  
842 appears wet biased) than the trade winds zones and the deep tropics. The amplitudes of the  
843 specific humidity interannual anomalies are also smaller by  $\sim 50\%$  (cf., figure S8) than those  
844 estimated over the trade winds zone and the deep tropics. The specific humidity interannual  
845 anomalies show the same degree of correlation ( $\sim 0.65$ ) with altitude as the one estimated in the  
846 trade winds zones, suggesting again that the strength of the convection defines the correlation  
847 strength of the specific humidity anomalies throughout the vertical extent of the troposphere.

848 Table S2 shows that ERA-Interim and UCAR (at all pressure levels) as well as AIRS (at 500  
849 hPa and 400 hPa) capture a moistening of the subtropics, except from the AIRS at 700 hPa and  
850 600 hPa pressure levels where the data set indicates a decrease in the SH over time. JPL does not  
851 show a decrease/increase of specific humidity with time, and MERRA shows moistening of the

852 middle troposphere. Compared to the deep tropics and the trade winds zones, [Table S2 shows](#)  
853 [that](#) the [mean](#) differences of the specific humidity values between JPL and the rest of the data  
854 sets are smaller than in the deep tropics and similar to the trade winds zone, except at the 400  
855 hPa where it remains almost the same. Again, this hints towards the notion that different data sets  
856 agree better with one another over regions characterized by less convection.

857 [Figure 3 \(bottom row\) and figure S3 show that the specific humidity climatologies in the](#)  
858 [subtropics in the middle troposphere show the exact same behavior as in the deep tropics and the](#)  
859 [trade winds zone at all pressure levels. Specifically, JPL captures moister air than all other data](#)  
860 [sets](#) and this wetness is more pronounced at 400 hPa. [The AIRS is systematically the driest](#)  
861 [among all climatologies](#) [and MERRA, ERA-Interim](#), and UCAR show an excellent agreement  
862 being in between the JPL and the AIRS data sets. [At 700 hPa, MERRA and UCAR are the](#)  
863 [wettest and driest climatologies respectively, with JPL, ERA-Interim, and AIRS having a very](#)  
864 [good agreement lying in between. At 600 hPa, JPL agrees very well with both reanalyses](#)  
865 [differing by < 2.0%, and UCAR agrees very well with AIRS being drier than](#) by ~7.0%. [All](#)  
866 [these differences are smaller than each data set's retrieval uncertainty, except that of](#) JPL at 400  
867 hPa which is > 30%. [Similar to the deep tropics and the trade winds zone, the specific humidity](#)  
868 [interannual anomalies in the subtropics exhibit the same behaviors being in excellent agreement](#)  
869 [with one another having almost the same median value, similar IQR, and similar scattering](#)  
870 [around the median \(cf., figure 4 – bottom row and figure S8\).](#)

871

### 872 [3.4. Differences between JPL and UCAR specific humidity retrievals](#)

873 [To begin establishing the RO-derived specific humidity as a climate product, we must](#)  
874 [investigate the origin of the observed differences between the JPL and UCAR specific humidity](#)

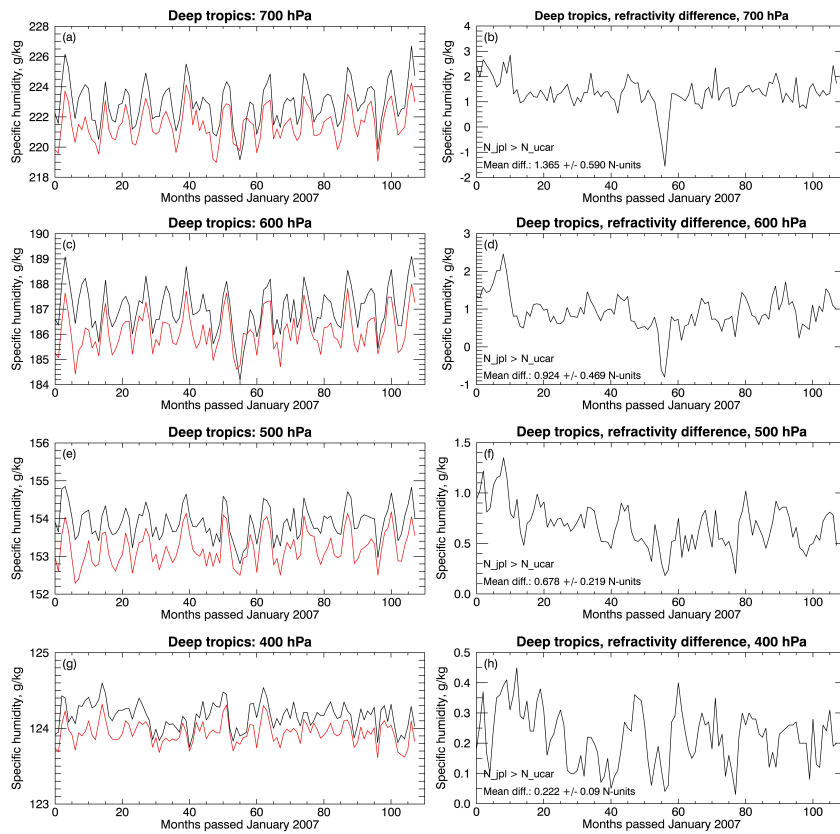
**Comment [18]:**

Reviewer #1. General Comment #2.

Reviewer #2. Minor Comment #13.

**Addressed and completed.**

875 statistics. One of the possible reasons for the observed discrepancies in figure 1 could be the  
876 difference in the refractivity products generated by each center. Here, we investigate this  
877 possibility by analyzing the JPL and UCAR refractivity climatologies in the deep tropics.  
878



879  
880 **Figure 5.** Times series of the monthly zonal averages of the refractivity from January 1, 2007  
881 until December 31, 2015 in the deep tropics ( $\pm 15^\circ$ ) from JPL (black) and UCAR (red) at (a) 700  
882 hPa, (b) 600 hPa, (c) 500 hPa, and (d) 400 hPa pressure levels. The time series of the refractivity  
883 differences between JPL minus UCAR are shown at (e) 700 hPa, (f) 600 hPa, (g) 500 hPa, and  
884 (h) 400 hPa.

885       Figure 5 shows that the monthly zonal averages of the JPL-derived refractivity are  
886       systematically larger than those estimated by UCAR and this is noticeable at all pressure levels.  
887       The JPL and UCAR climatologies are in excellent agreement, which becomes better with  
888       increasing altitude. Interestingly, we notice a sharp dip in the JPL refractivity in figure 5 during  
889       the summer of 2011 at 700 hPa and 600 hPa, which explains the JPL specific humidity  
890       interannual anomaly dip during the same period at 700 hPa and 600 hPa in figure 2.  
891       Quantitatively, the 9-year mean differences are  $1.365 \pm 0.590$  N-units (or 0.6% with respect to  
892       UCAR) at 700 hPa,  $0.924 \pm 0.469$  N-units (or 0.5% with respect to UCAR) at 600 hPa,  
893        $0.678 \pm 0.217$  N-units (or 0.4% with respect to UCAR) at 500 hPa, and  $0.222 \pm 0.09$  N-units (or  
894       0.2% with respect to UCAR) at 400 hPa. From equation (1), we can derive an expression that  
895       relates refractivity changes into water vapor pressure changes, assuming a constant temperature:  
896

$$\delta N \equiv (N' - N) = a \cdot \frac{P}{T} + b \cdot \frac{(e + \delta e)}{T^2} - a \cdot \frac{P}{T} - b \cdot \frac{e}{T^2} = \frac{b}{T^2} \cdot \delta e \Leftrightarrow \frac{\delta N}{\delta e} = \frac{b}{T^2} \quad [3]$$

897  
898       Where  $\delta N$  and  $\delta e$  represent the refractivity and water vapor pressure changes. We convert these  
899       water vapor changes into specific humidity changes using equation (2). The mean refractivity  
900       differences from figure 5 correspond to specific humidity differences of the order of: a)  
901        $0.26 \pm 0.11$  g kg<sup>-1</sup> at 700 hPa, b)  $0.19 \pm 0.10$  g kg<sup>-1</sup> at 600 hPa, c)  $0.16 \pm 0.05$  g kg<sup>-1</sup> at 500 hPa, and  
902       d)  $0.06 \pm 0.02$  g kg<sup>-1</sup> at 400 hPa. Comparing these values with the mean differences in Table 1, we  
903       argue that the majority of the specific humidity differences between JPL and UCAR at all  
904       pressure levels results from the refractivity differences between the two centers.

905       Another factor that could cause the JPL and UCAR specific humidity climatologies to  
906       deviate is the different retrieval approaches adopted by JPL and UCAR. JPL uses equation (1) to

907 solve for the water vapor pressure by assuming a background temperature from the ECMWF  
908 TOGA operational analysis. Comparisons of ECMWF operational products with rawinsondes  
909 over the Pacific and Indian oceans reveal a systematic warm bias in the operational analysis of  
910 the order of 0.5 K with an RMSE of 1.0 K [Nuret and Chong, 1996; Nagarajan and Aiyer,  
911 2004]. This bias leaks through the JPL retrievals, causing JPL to overestimate the specific  
912 humidity (e.g., by  $\sim 0.10 \text{ g kg}^{-1}$  at 500 hPa and 400 hPa). UCAR uses a variational assimilation  
913 approach that takes ERA-Interim temperature and humidity information as *a-priori*. This could  
914 explain why UCAR climatologies appear to be consistent with ERA-Interim at all altitudes in  
915 the deep tropics and in the middle troposphere at the trade winds zone and the subtropics.  
916 Additionally, the different quality control used by the two centers leads to a different number of  
917 available occultations, which could also introduce a small bias in the specific humidity  
918 comparisons. However, this effect would be small as we analyze monthly zonal averages.  
919

**Comment [19]:**

Reviewer #1. Specific Comment #6.

Addressed and completed.

#### 920 4. Conclusions

921 Based on statistical tests using a 2-sigma uncertainty and 95% confidence level criteria  
922 the RO observations agree very well with the MERRA, ERA-Interim, and AIRS climatologies  
923 by capturing similar magnitudes and patterns of variability in the monthly zonal mean specific  
924 humidity and interannual anomaly over annual and interannual timescales. The specific humidity  
925 differences between RO and all other climatologies fall within the expected specific humidity  
926 retrieval uncertainty. The JPL and UCAR specific humidity climatologies differ by less than  
927 15% in the median (depending on location and pressure level) and these differences are primarily  
928 due to the differences in the retrieved refractivity. Although we could explain these differences,  
929 we cannot speculate which center is closer to the truth, we demonstrate that both JPL and UCAR

**Comment [20]:**

Reviewer #1. General Comment #2.

Addressed and completed.

930 essentially provide similar specific humidity climatologies within the retrieval uncertainty. At  
931 500 hPa and 400 hPa, in all climate zones, JPL appears to be the wettest of all data sets; AIRS is  
932 the driest of all data sets, and UCAR, ERA-Interim, and MERRA are in very good agreement  
933 lying in between the JPL and AIRS climatologies. In the lower-to-middle troposphere, we  
934 present a complex behavior of discrepancies, as we speculate that this might be because the 700  
935 hPa and 600 hPa pressure levels are closest to the planetary boundary layer that interfaces with  
936 the free troposphere via convection and entrainment. This implies that the specific humidity  
937 measured by each data set could be susceptible to the degree which each data set represents this  
938 vertical coupling. Weather models are known to be less accurate over convective regions, and  
939 recent studies indicate that RO observations could be positively biased by only 2% over cloudy  
940 regions [Yang and Zou, 2017].

**Comment [21]:**

Reviewer #1. Specific Comment #9.  
Addressed and completed.

941 Given the above, the RO observations could augment the reanalyses and satellite  
942 observations by providing an ~~independent additional complementary~~ data set to study short-term  
943 SH variations, which are critical to the study of water vapor trends, and climate sensitivity,  
944 variability, and change. More detailed statistical analysis is required between the SH products  
945 between different RO processing centers to define its structural uncertainty. The reduced daily  
946 sampling of the COSMIC mission may be also a limiting factor in properly establishing  
947 differences between the RO and other platforms. We expect that the increased sampling rate of  
948 the COSMIC-2 follow-on mission will provide a much better picture of the tropical and  
949 subtropical climatology, which will help us extend the current short-term RO record.

**Comment [23]:**

Reviewer #2. Minor Comment #15.  
Addressed and completed.

**Comment [24]:**

Reviewer #2. Minor Comment #17.  
Addressed and completed.

950  
951  
952

953 **Acknowledgments:**

954 This research was carried out at the Jet Propulsion Laboratory, California Institute of  
955 Technology, under a contract with the National Aeronautics and Space Administration Earth  
956 Science Mission Directorate (SMD). We thank Robert Khachikyan for making publicly available  
957 the JPL-RO retrievals through the AGAPE interactive search tool. We would like to  
958 acknowledge the University Corporation for Atmospheric Research (UCAR) COSMIC Data  
959 Analysis and Archive Center (CDAAC) for making publicly available the COSMIC data sets.

960 We would like to thank NASA Earth Observing System Data and Information System (EOSDIS)

961 for making publicly available the MERRA and AIRS data sets. [The RO SH products are publicly](#)  
962 [available through JPL Global Environmental & Earth Science Information System \(GENESIS\)](#)  
963 [portal at `ftp://genesis.jpl.nasa.gov/pub/genesis/glevels/cosmic?postproc`, as well as accessible via](#)  
964 [the publicly available Atmospheric Grid Analysis and Extraction Profile \(AGAPE\) web interface](#)  
965 [at `https://genesis.jpl.nasa.gov/agape/`. The AIRS/AMSU v6 Level-3 SH products are described in](#)  
966 [detail in \*Tian et al. \[2013\]\*, and for our analysis we use the AIRX3STM v006 data downloadable](#)  
967 [from multiple different online tools, including the Simple Subset Wizard \(SSW\) at](#)  
968 [`https://disc.gsfc.nasa.gov/SSW/` and the Mirador search base at `https://mirador.gsfc.nasa.gov/`.](#)  
969 [From the MERRA SH products we use are the MAIMNPANA v5.2.0 files, which we](#)  
970 [downloaded from the SSW. The ERA-Interim SH products are publicly available at](#)  
971 [`http://apps.ecmwf.int/datasets/data/interim-full-mod4/levtype=sfc/`.](#)

**Comment [25]:**

Reviewer #2. Minor Comment #10.

Addressed and completed.

972

973

974

976 **References:**

977 Anthes, R. A., et al. (2008), The COSMIC/FORMOSAT-3 mission: Early results, *Bull. Am. Meteorol. Soc.*, **89**, pp. 313–333, doi:10.1175/BAMS-89-3-313

979 Ao, C. O., T. K. Meehan, G. A. Hajj, A. J. Mannucci, and G. Beyerle (2003), Lower troposphere  
980 refractivity bias in GPS occultation retrievals, *J. Geophys. Res.*, **108**(D18), 4577,  
981 doi:10.1029/2002JD003216

982 [Ao, C. O., D. E. Waliser, S. K. Chan, J.-L. Li, B. Tian, F. Xie, and A. J. Mannucci \(2012\),](#)  
983 [Planetary boundary layer heights from GPS radio occultation refractivity and humidity](#)  
984 [profiles, J. Geophys. Res., 117, D16117, doi:10.1029/2012JD017598](#)

985 Blackwell, W. J., M. Pieper, and L. G. Jairam (2008), Neural network estimation of atmospheric  
986 profiles using AIRS/IASI/AMSU data in the presence of clouds, *Proc of SPIE*, 7149,  
987 doi:10.1117/12.804841

988 [Bosilovich, M. G., F. R. Robertson, L. Takacs, A. Molod, and D. Mocko \(2017\), Atmospheric](#)  
989 [Water Balance and Variability in the MERRA-2 Reanalysis, J. Clim., 30, pp. 1177–1196,](#)  
990 [doi:10.1175/JCLI-D-16-0338.1](#)

991 Chen, J., A. D. Del Genio, B. E. Carlson, and M. G. Bosilovich (2008), The spatiotemporal  
992 structure of twentieth-century climate variations in observations and reanalyses. Part I:  
993 Long-term trend., *J. Clim.*, **21**, pp. 2611–2633, doi:10.1175/2007JCLI2011.1

994 Chuang, H., X. Huang, and K. Minschwaner (2010), Interannual variations of tropical upper  
995 tropospheric humidity and tropical rainy-region SST: Comparisons between models,  
996 reanalyses, and observations, *J. Geophys. Res.*, **115**, D21125,  
997 doi:10.1029/2010JD014205

998 Collard, A. D., and S. B. Healy (2003), The combined impact of future space-based atmospheric

999 sounding instruments on numerical weather prediction analysis fields: A simulation  
1000 study, *Q. J. R. Meteorol. Soc.*, **129**, pp. 2741–2760

1001 Dee, D. P., Uppala, S. M., Simmons, A. J., Berrisford, P., Poli, P., Kobayashi, S., Andrae, U.,  
1002 Balmaseda, M. A., Balsamo, G., Bauer, P., Bechtold, P., Beljaars, A. C. M., van de Berg,  
1003 L., Bidlot, J., Bormann, N., Delsol, C., Dragani, R., Fuentes, M., Geer, A. J., Haimberger,  
1004 L., Healy, S. B., Hersbach, H., Hólm, E. V., Isaksen, L., Källberg, P., Köhler, M.,  
1005 Matricardi, M., McNally, A. P., Monge-Sanz, B. M., Morcrette, J.-J., Park, B.-K.,  
1006 Peubey, C., de Rosnay, P., Tavolato, C., Thépaut, J.-N. and Vitart, F. (2011), The ERA  
1007 Interim reanalysis: configuration and performance of the data assimilation system, *Q.J.R.*  
1008 *Meteorol. Soc.*, **137**, pp. 553–597. doi:10.1002/qj.828

1009 Dolinar, E. K., X. Dong, and B. Xi (2016), Evaluation and intercomparison of clouds,  
1010 precipitation, and radiation budgets in recent reanalyses using satellite-surface  
1011 observations, *Clim. Dyn.*, **46**, pp. 2123–2144, doi: 10.1007/s00382-015-2693-z

1012 Fasullo, J. T., and K. E. Trenberth (2012), A less cloudy future: The role of subtropical  
1013 subsidence in climate sensitivity, *Science*, **338**, pp. 792–794,  
1014 doi:10.1126/science1227465

1015 Flato, G., J. Marotzke, B. Abiodun, P. Braconnot, S.C. Chou, W. Collins, P. Cox, F. Driouech,  
1016 S. Emori, V. Eyring, C. Forest, P. Gleckler, E. Guilyardi, C. Jakob, V. Kattsov, C.  
1017 Reason and M. Rummukainen, 2013: Evaluation of Climate Models. In: Climate Change  
1018 2013: The Physical Science Basis. Contribution of Working Group I to the Fifth  
1019 Assessment Report of the Intergovernmental Panel on Climate Change [Stocker, T.F., D.  
1020 Qin, G.-K. Plattner, M. Tignor, S.K. Allen, J. Boschung, A. Nauels, Y. Xia, V. Bex and  
1021 P.M. Midgley (eds.)]. Cambridge University Press, Cambridge, United Kingdom and

1022 New York, NY, USA

1023 Fetzer, E. J., B. H. Lambrigtsen, A. Eldering, H. H. Aumann, and M. T. Chahine (2006), Biases  
1024 in total precipitable water vapor climatologies from Atmospheric Infrared Sounder and  
1025 Advanced Microwave Scanning Radiometer, *J. Geophys. Res.*, **111**, D09S16,  
1026 doi:10.1029/2005JD006598

1027 Fetzer, E. J., et al. (2008), Comparison of upper tropospheric water vapor observations from the  
1028 Microwave Limb Sounder and Atmospheric Infrared Sounder, *J. Geophys. Res.*, **113**,  
1029 D22110, doi:10.1029/2008JD010000

1030 Frenkel, Y., A. J. Majda, and B. Khouider (2012), Using the Stochastic Multicloud Model  
1031 to Improve Tropical Convective Parameterization: A Paradigm Example, *J. Atmos.*  
1032 *Sci.*, **69**, pp. 1080–1105

1033 Gorbunov, M. E., A. V. Shmakov, S. S. Leroy, and K. B. Lauritsen (2011), COSMIC Radio  
1034 Occultation Processing: Cross-Center Comparison and Validation, *J. Atmos. Oceanic*  
1035 *Technol.*, **28**, pp. 737–751, doi:<http://dx.doi.org/10.1175/2011JTECHA1489.1>

1036 Hannay, C., et al. (2009), Evaluation of forecasted southeast Pacific stratocumulus in the NCAR,  
1037 GFDL, and ECMWF models, *J. Clim.*, **22**, pp. 2871–2889, doi:10.1175/2008JCLI2479.1

1038 Hearty, T. J., A. Savtchenko, B. Tian, E. Fetzer, Y. L. Yung, M. Theobald, B. Vollmer, E.  
1039 Fishbein, and Y.-I. Won (2014), Estimating sampling biases and measurement  
1040 uncertainties of AIRS/AMSU-A temperature and water vapor observations using  
1041 MERRA reanalysis, *J. Geophys. Res. Atmos.*, **119**, pp. 2725–2741,  
1042 doi:10.1002/2013JD021205

1043 Hegerl, G. *et al.* (2015), Challenges in quantifying changes in the global water cycle, *Bull. Amer.*  
1044 *Meteor. Soc.*, **96**, pp. 1097–1115

1045 Ho, S.-P., Y.-H. Kuo, and S. Sokolovskiy (2007), Improvement of the temperature and moisture  
1046 retrievals in the lower troposphere using AIRS and GPS radio occultation measurements,  
1047 *J. Atmos. Oceanic Technol.*, **24**, pp. 1726–1737, doi:10.1175/JTECH2071.1

1048 Ho, S.-P., X. Zhou, Y.-H. Kuo, D. Hunt, and J.-H. Wang (2010), Global Evaluation of  
1049 Radiosonde Water Vapor Systematic Biases using GPS Radio Occultation from COSMIC  
1050 and ECMWF Analysis, *Remote Sens.*, **2**(5), pp. 1320–1330, doi:10.3390/rs2051320

1051 Holloway, C. E., and J. D. Neelin (2009), Moisture vertical structure, column water vapor, and  
1052 tropical deep convection, *J. Atmos. Sci.*, **66**, pp. 1665–1683,  
1053 doi:<http://dx.doi.org/10.1175/2008JAS2806.1>

1054 Jiang, J.H., et al. (2012), Evaluation of Cloud and Water Vapor Simulations in IPCC AR5  
1055 Climate Models Using NASA “A-Train” Satellite Observations, *J. Geophys. Res.*,  
1056 **117**, D14105, doi:10.1029/2011JD017237

1057 Kahn, B. H., F. W. Irion, V. T. Dang, E. M. Manning, S. L. Nasiri, C. M. Naud, J. M. Blaisdell,  
1058 M. M. Schreier, Q. Yue, K. W. Bowman, E. J. Fetzer, G. C. Hulley, K. N. Liou, D.  
1059 Lubin, S. C. Ou, J. Susskind, Y. Takano, B. Tian, and J. R. Worden (2014), The  
1060 Atmospheric Infrared Sounder version 6 cloud products, *Atmos. Chem. Phys.*, **14**,  
1061 pp. 399–426, doi:<https://doi.org/10.5194/acp-14-399-2014>

1062 Kishore, P., M. Venkat Ratnam, S. P. Namboothiri, I. Velicogna, G. Basha, J. H. Jiang,  
1063 K. Igarashi, S. V. B. Rao, and V. Sivakumar (2011), Global (50S–50N) distribution of  
1064 water vapor observed by COSMIC GPS RO: Comparison with GPS radiosonde, NCEP,  
1065 ERA Interim, and JRA-25 reanalysis datasets, *JASTP*, **73**(13), pp. 1849–1860

1066 Kuo, Y.-H., W. S. Schreiner, J. Wang, D. L. Rossiter, and Y. Zhang (2005), Comparison of GPS  
1067 radio occultation soundings with radiosondes, *Geophys. Res. Lett.*, **32**, L05817,

1068 doi:10.1029/2004GL021443

1069 Kursinski, E. R., and T. Gebhardt (2014), A Method to Deconvolve Errors in GPS RO-Derived  
1070 Water Vapor Histograms, *J. Atmos. Ocean. Technol.*, **31**, pp. 2606–2628,  
1071 doi:10.1175/JTECH-D-13-00233.1

1072 Kursinski, E. R., G. A. Hajj, J. T. Schofield, R. P. Linfield, and K. R. Hardy (1997), Observing  
1073 Earth's atmosphere with radio occultation measurements using the Global Positioning  
1074 System, *J. Geophys. Res.*, **102**(D19), pp. 23,429–23,465, doi:10.1029/97JD01569

1075 Kursinski, E. R., and G. A. Hajj (2001), A comparison of water vapor derived from GPS  
1076 occultations and global weather analyses, *J. Geophys. Res.*, **106**(D1), pp. 1113–1138,  
1077 doi:10.1029/2000JD900421

1078 [Nagarajan, B., and A. R. Aiyyer \(2004\), Performance of the ECMWF Operational Analyses over](#)  
1079 [the Tropical Indian Ocean, \*Mon. Weath. Rev.\*, \*\*132\*\*, pp. 2275–2282,](#)  
1080 [doi:10.1175/1520-0493\(2004\)132<2275:POTEAO>2.0.CO;2](#)

1081 [Nuret, M., and M. Chong \(1996\), Monitoring the performance of the ECMWF operational](#)  
1082 [analysis using the enhanced TOGA COARE observational network, \*Wea. Forecasting\*,](#)  
1083 [11, pp. 53–65, doi:10.1175/1520-0434\(1996\)011<0053:MTPOTE>2.0.CO;2](#)

1084 Read, W. G., et al. (2007), Aura Microwave Limb Sounder upper tropospheric and lower  
1085 stratospheric H<sub>2</sub>O and relative humidity with respect to ice validation, *J. Geophys.*  
1086 *Res.*, **112**, D24S35, doi:10.1029/2007JD008752

1087 Rienecker, M. M., M. J. Suarez, R. Todling, J. Bacmeister, L. Takacs, H.-C. Liu, W. Gu,  
1088 M. Sienkiewicz, R. D. Koster, R. Gelaro, I. Stajner, and J.E. Nielsen (2008), The  
1089 GOES-5 Data Assimilation System – Documentation of versions 5.0.1, 5.1.0, and  
1090 5.2.0, *NASA Tech. Rep.*, Series on Global Modeling and Data Assimilation,

1091 NASA/TM-2008-104606, **27**, 92 p.

1092 Rienecker, M. M., and Coauthors (2011), MERRA: NASA's Modern-Era Retrospective  
1093 Analysis for Research and Applications. *J. Climate*, **24**, pp. 3624–3648,  
1094 doi: <http://dx.doi.org/10.1175/JCLI-D-11-00015.1>

1095 Schreier, M. M., B. H. Kahn, K. Sušelj, J. Karlsson, S. C. Ou, Q. Yue, and S. L. Nasiri (2014),  
1096 Atmospheric parameters in a subtropical cloud regime transition derived by AIRS and  
1097 MODIS: observed statistical variability compared to ERA-Interim, *Atmos. Chem. Phys.*,  
1098 **14**, pp. 3573–3587

1099 Sherwood, S. C., R. Roca, T. M. Weckwerth, and N. G. Andronova (2010), Tropospheric water  
1100 vapor, convection, and climate, *Rev. Geophys.*, **48**, RG2001,  
1101 doi:10.1029/2009RG000301

1102 Simmons, A. J., and A. Hollingsworth (2002), Some aspects of the improvement in skill of  
1103 numerical prediction, *Q. J. R. Meteorol. Soc.*, **128**, pp. 647–677

1104 Simmons, A. J., M. Hortal, G. Kelly, A. McNally, A. Untach, and S. Uppala (2005), ECMWF  
1105 analyses and forecasts of stratospheric winter polar vortex breakup: September 2002 in  
1106 the southern hemisphere and related events, *J. Atmos. Sci.*, **62**, pp. 668–689

1107 Simmons, A. J., Poli, P., Dee, D. P., Berrisford, P., Hersbach, H., Kobayashi, S. and Peubey, C.  
1108 (2014), Estimating low-frequency variability and trends in atmospheric temperature using  
1109 ERA-Interim, *Q. J. R. Meteorol. Soc.*, **140**, pp. 329–353, doi:10.1002/qj.2317

1110 [Sokolovskiy, S., C. Rocken, D. Hunt, W. Schreiner, J. Johnson, D. Masters, and S. Esterhuizen](#)  
1111 [\(2006\), GPS profiling of the lower troposphere from space: Inversion and demodulation](#)  
1112 [of the open-loop radio occultation signals, Geophys. Res. Lett.](#), **33**, L14816,  
1113 doi:10.1029/2006GL026112

1114 | [Takacs, L. L., M. Suarez, and R. Todling \(2016\), Maintaining atmospheric mass and water](#)  
1115 | [balance in reanalyses, \*Quart. J. Roy. Meteor. Soc.\*, \*\*142\*\*, 1565–1573, doi:10.1002/qj.2763](#)

1116 | Tian, B., E. J. Fetzer, B. H. Kahn, J. Teixeira, E. Manning, and T. Hearty (2013), Evaluating  
1117 | CMIP5 Models using AIRS Tropospheric Air Temperature and Specific Humidity  
1118 | Climatology, *J. Geophys. Res. Atmos.*, **118**, 114–134, doi:10.1029/2012JD018607

1119 | Vergados, P., A. J. Mannucci, and C. O. Ao (2014), Assessing the performance of GPS radio  
1120 | occultation measurements in retrieving tropospheric humidity in cloudiness: A  
1121 | comparison study with radiosondes, ERA-Interim, and AIRS data sets, *J. Geophys. Res.*  
1122 | *Atmos.*, **119**, pp. 7718–7731, doi:10.1002/2013JD021398

1123 | Vergados, P., A. J. Mannucci, C. O. Ao, J. H. Jiang, and H. Su (2015), On the comparisons of  
1124 | tropical relative humidity in the lower and middle troposphere among COSMIC radio  
1125 | occultations and MERRA and ECMWF data sets, *Atmos. Meas. Tech.*, **8**, pp. 1789–1797,  
1126 | doi:<https://doi.org/10.5194/amt-8-1789-2015>

1127 | Wang, H., and W. Su (2013), Evaluating and understanding top of the atmosphere cloud  
1128 | radiative effects in Intergovernmental Panel on Climate Change (IPCC) Fifth Assessment  
1129 | Report (AR5) Coupled Model Intercomparison Project Phase 5 (CMIP5) models using  
1130 | satellite observations, *J. Geophys. Res. Atmos.*, **118**, pp. 683–699,  
1131 | doi:10.1029/2012JD018619

1132 | Wang, B. R., X.-Y. Liu, and J.-K. Wang (2013), Assessment of COSMIC radio occultation  
1133 | retrieval product using global radiosonde data, *Atmos. Meas. Tech.*, **6**, pp. 1073–1083,  
1134 | doi:10.5194/amt-6-1073-2013

1135 | Waters et al. (2006), The Earth Observing System Microwave Limb Sounder (EOS MLS) on the  
1136 | Aura Satellite, *IEEE Trans. Geosci. Remote Sens.*, **44**, pp. 1075–1092

1137 Wu, W.-S., R.J. Purser, and D.F. Parrish (2002), Three-dimensional variational analysis with  
1138 spatially inhomogeneous covariances, *Mon. Wea. Rev.*, **130**, pp. 2905–2916  
1139 [Xie, F., D. L. Wu, C. O. Ao, E. R. Kursinski, A. J. Mannucci, and S. Syndergaard \(2010\), Super](#)  
1140 [refraction effects on GPS radio occultation refractivity in marine boundary](#)  
1141 [layers, \*Geophys. Res. Lett.\*, \*\*37\*\*, L11805, doi:10.1029/2010GL043299](#)

1142 [Yang, S. and X. Zou \(2017\), Dependence of positive refractivity bias of GPS RO cloudy profiles](#)  
1143 [on cloud fraction along GPS RO limb tracks, \*GPS Solut.\*, \*\*21\*\*, pp. 499–509,](#)  
1144 [doi:10.1007/s10291-016-0541-1](#)